HHS Public Access

Author manuscript

Supercond Sci Technol. Author manuscript; available in PMC 2018 February 01.

Published in final edited form as:

Supercond Sci Technol. 2017 February ; 30(2): . doi:10.1088/1361-6668/30/2/024011.

A persistent-mode 0.5 T solid-nitrogen-cooled MgB2 magnet for MRI

Jiayin Ling[1,2], **John P. Voccio**[1,3], **Seungyong Hahn**[1,4], **Timing Qu**[1,5], **Juan Bascuñán**[1], and **Yukikazu Iwasa**[1]

[1]Francis Bitter Magnet Lab, Plasma Science and Fusion Center, Massachusetts Institute Technology, 170 Albany St, Cambridge, MA 02139, USA

[2]GE Healthcare, 3001 W Radio Dr, Florence, SC 29501, USA

[3]Wentworth Institute of Technology, 550 Huntington Ave, Boston, MA 02115, USA

[4]National High Magnetic Field Laboratory, Florida State University, 2031 E Paul Dirac Dr, Tallahassee, FL 32310, USA

[5]Department of Mechanical Engineering, Tsinghua University, 30 Shuangqing Rd, Haidian, Beijing 100084, China

Abstract

This paper presents construction details and test results of a persistent-mode 0.5-T MgB_2 magnet developed at the Francis Bitter Magnet Lab, MIT. The magnet, of 276-mm inner diameter and 290-mm outer diameter, consisted of a stack of 8 solenoidal coils with a total height of 460 mm. Each coil was wound with monofilament MgB_2 wire, equipped with a persistent-current switch and terminated with a superconducting joint, forming an individual superconducting loop. Resistive solder joints connected the 8 coils in series. The magnet, after being integrated into a testing system, immersed in solid nitrogen, was operated in a temperature range of 10–13 K. A two-stage cryocooler was deployed to cool a radiation shield and the cold mass that included mainly ~60 kg of solid nitrogen and the magnet. The solid nitrogen was capable of providing a uniform and stable cryogenic environment to the magnet. The magnet sustained a 0.47-T magnetic field at its center persistently in a range of 10–13 K. The current in each coil was inversely calculated from the measured field profile to determine the performance of each coil in persistent-mode operation. Persistent-current switches were successfully operated in solid nitrogen for ramping the magnet. They were also designed to absorb magnetic energy in a protection mechanism; its effectiveness was evaluated in an induced quench.

Keywords

MgB_2; MRI magnet; persistent mode; solid nitrogen

1. Introduction

Medical imaging is critical for quality health care for early detection and efficient treatment of disease and injury. Magnetic resonance imaging (MRI) has become one of the major noninvasive diagnostic imaging tools today. An MRI system requires a strong, uniform and

stable magnetic field for imaging, thus a magnet is an essential component of an MRI system. Due to high current density and zero Joule heating, superconductors have been selected as the only type of conductor for making >1 T MRI magnets.

MRI magnet manufacturers rely chiefly on Niobium Titanium (NbTi) because of its low (compared with other superconductors) manufacturing cost and ease of handling. NbTi, despite its relatively low critical temperature of only 9.2 K, has been used for MRI magnet fabrication since the 1970's. Because of the critical temperature, an NbTi magnet is typically operated at liquid helium (LHe) boiling point of 4.2 K. For high operation stability, nowadays, most of commercial MRI magnets are operated in a bath of ~2000-litter LHe. Unfortunately, the price of helium as shown in Figure 1, a nonrenewable resource, has been surging since the beginning of this century. Even in the US, the biggest helium producer in the world, gaseous helium costs three times more than it did in the beginning of this century [1]. Outside the US, particularly in China, India, Middle East, and South America where MRI markets are emerging, helium is even more expensive. Under this new circumstance, NbTi MRI magnet operated in an LHe bath may no longer remain the most viable option, prompting MRI magnet manufacturers to seriously consider low-LHe or even LHe-free options for MRI magnets.

1.1. MgB_2

Discovered in 2001 [2], a high temperature superconductor (HTS) of magnesium diboride (MgB_2) with a critical temperature of 39 K has spurred intensive R&D efforts [3–18]. For applications below 3 T, the high critical temperature immunizes MgB_2 wires against premature quench and allows MgB_2 magnets—much more easily than NbTi magnets—for LHe-free operation, making MgB_2 a viable and promising competitor to NbTi. For example, an MgB_2 magnet can be operated in solid nitrogen (SN2) in a temperature range of 10–20 K [19–22]. Note that in the 10–20 K range, SN2 enthalpy density is >10 times greater than those of metals, making an MgB_2-SN2 system operating in this range to possess a thermal mass density far greater than that of a conduction-cooled system. Together with relatively large thermal diffusivities in the 10–20 K range [23], SN2 can effectively anchor the temperature of the MgB_2 magnet. Even without SN2, MgB_2 operated in the 10–20 K range will be more stable than NbTi at 4.2 K, simply because of its higher critical temperature and higher enthalpy density compared with those of NbTi.

One of the biggest challenges with MgB_2 is to make reliable superconducting joints. An MRI magnet needs to provide a spatially uniform and temporally stable magnetic field. For a whole-body MRI magnet, its field variations are typically less than 10 part-per-million (ppm) of the center field over a 50-cm diameter spherical volume (DSV) and 0.1 ppm over a scan that lasts ~30 min [24–26]. If such a magnet is driven by a power supply, the power supply requires the same level of temporal stability. Such an ultra-stable power supply would add a significant amount to the cost of an MRI system. Moreover, a power supply requires current leads that would bring enormous heat into the cryogenic environment of a magnet. Therefore, all commercial NbTi MRI magnets are equipped with superconducting joints to allow operation in persistent mode. Once such a magnet is energized, its superconducting coils and joints can sustain a persistent current independent of a power supply. However,

superconducting splicing techniques, though relatively easy with NbTi wires, proved to be challenging with MgB_2 wires.

The MIT Francis Bitter Magnet Laboratory (FBML) has been working since 2008 toward persistent-mode operation of an MgB_2 magnet [12–18]. By the end of 2015, an MgB_2 magnet of a nominal 0.5-T center field and 240-mm warm bore was completed and operated persistently in SN2 in a temperature range of 10–13 K [27]. The experimental and operational details of the magnet is presented in the paper.

2. Experimental details

2.1. Wire selection

A persistent-mode superconducting magnet requires a technique to make superconducting splices. Before 2010, the team at MIT developed a technique to splice multifilament MgB_2 wires [13,14]. Later, this splicing technique was proven much more repeatable with monofilament MgB_2 wires [15,16]. In order to reduce the risk of making underperformed joints, the team decided to wind the magnet with monofilament MgB_2 wires that can be spliced more reliably.

Flux-jumping, in 1960's caused premature quench in magnets wound with monofilament NbTi conductors, is not an issue for magnets wound with monofilament MgB_2 conductors. Chiefly because MgB_2 has a higher critical temperature than NbTi, its flux-jumping-free filament size, <1 mm for use in this magnet [28], is much bigger than that of NbTi.

The MgB_2 wire used in this magnet was produced by the Hyper Tech Research, Inc. in Columbus, Ohio. A photograph of a bare wire cross-section is shown in Figure 2. The Φ0.84-mm bare monofilament MgB_2 wire consists, from innermost to outermost, of a Φ0.4-mm MgB_2 core, a 70-μm barrier layer of niobium to enclose MgB_2, a 100-μm layer of copper, and a 45-μm layer of Monel to provide mechanical strength. The copper layer takes about 35% of the total cross-sectional area of the wire. The copper to superconductor ratio of the wire was chosen such that a wire carrying 100 A at 10 K would have ~5 s before heated to 300 K adiabatically. The wire diameter is 1.0 mm with S-glass insulation.

The wire has critical currents (I_c's) measured at the FBML of >400 A at 10 K and >200 A at 20 K in self-field—about 0.1 T at 200 A and 0.2 T at 400 A, respectively. Other electromagnetic properties of the wire may be found in literature [29,30]. Short samples and a small coil wound with the wire were tested to ensure that the monofilament wire was flux-jumping-free [28].

2.2. Electromagnetic design

The splicing technique has been developed at the FBML to work with both unreacted and reacted monofilament MgB_2 wires. When it is applied to unreacted wires, however, it involves a simpler procedure and results in higher I_c's than that applied to reacted wires. Therefore, we adopted the wind-and-react procedure: wind the magnet with unreacted MgB_2 wires and make joints before heat treating the whole coil-joint module.

The wind-and-react procedure, though worked fine for the dedicated MRI magnet, may be cost-ineffective for whole-body MRI magnet manufacturers. The procedure requires coil mandrel and wire insulation withstanding a heat treatment temperature >700°C—far beyond safe temperatures for mandrel and insulation materials of most existing MRI magnets. A furnace to cope with the heat treatment can also be quite expensive to build, operate and maintain. When the cost factor drives, a react-and-wind procedure may be desired for coil production.

As MgB_2 magnet technology is yet to become mature, imperfections could be introduced to coils during any stages of heat treatment, handling and testing. A magnet generating 0.5-T field uniformly over a 12-cm DSV requires kilometers of MgB_2 wire—a length too risky to be processed at a single time. In order to limit any imperfections within individual coils rather than letting them spoil the whole magnet, we decided to equip each coil with a persistent-current switch (PCS), terminate it with a superconducting joint and heat treat each coil-PCS-joint module individually. The coil modules would then be connected with resistive solder joints. This process also provided us the opportunity to replace underperformed coil modules with healthy spare ones to keep the entire magnet intact. On the other hand, with modular approach, multiple PCS's would add manufacturing costs to a magnet; later when ramping the magnet, they would also complicate the ramping procedure and bring excessive heating power into the cryogenic environment. So, this modular approach was perfect for this magnet, but it may not be the best option for commercial whole-body MRI magnets when MgB_2 magnet technology matures.

A schematic drawing of the magnet is shown in Figure 3, and the key electromagnetic parameters of the magnet are provided in Table 1. It consists of 8 coil modules, each containing wire <300 m. The magnet totally consumed 2.1-km long monofilament MgB_2 wires. Each coil has a winding inner diameter of 276 mm and an outer diameter of 290 mm. The total magnet height is 460 mm, including seven gaps—each 14–30 mm wide—between adjacent modules to mitigate the spatial field error. At 102 A, the magnet generates a center field of 0.5 T and at the same time a peak field of 0.7 T on its inner wall. A peak-to-peak field error in a 12-cm DSV is computed to be smaller than 200 ppm.

We recognized that a commercial MRI magnet is often designed to have 6–8 sub-coils as main and correction coils to bring the nominal field error in its DSV <1 ppm. However, to manage the potential risk in heat treatment and consider the conductor piece length that was available at the moment of the design, the magnet was designed in such a "modular" way, where a total of 8 coils were placed on the same inner diameter and the conductor length was <300 m in each coil.

Figure 4 shows a circuit diagram of the 8 coil modules of the magnet. Each coil was connected to its adjacent coils—or to a power supply at either end—via its two current terminals. These inter-coil connections, different from the superconducting joint in each coil, were resistive. When ramping up and down the magnet, we opened all the 8 PCS's—putting each PCS into resistive mode—so the 8 coils were connected in series effectively, as shown in Figure 4(a). When the magnet was ramped to the target current, we closed all the PCS's and then gradually ramped down the power supply. A persistent current was then sustained

in each coil, as shown by the dashed green lines in Figure 4(b). Though the connections between the coils were resistive (dashed orange lines), they did not affect persistent current in each individual superconducting loop, keeping the magnet in persistent mode.

In driven mode, the coils were effectively connected in series, so the magnet as a whole had a single self-inductance. In persistent mode, each coil operated independently, so the self-inductance of each coil, together with mutual inductance between each pair of coils, determined the current changing rate of each coil. This magnet was designed upon the assumption that all the MgB_2 joints were superconducting, so that the current in each coil would keep constant in persistent mode. If there had been any resistance in a coil or a joint, the current in the corresponding coil would decay and result in unbalanced current distribution among coils and thus a distorted field profile.

2.3. Cryogen selection

In the absence of LHe, an LHe-free magnet, comprising materials all of relatively low heat capacities even at 20 K, has practically no thermal mass. For thermally stable operation, it is desirable to enhance the thermal mass of an LHe-free superconducting magnet.

Figure 5, data from [23], plots the heat capacities of selected materials that are commonly considered as thermal mass enhancers. SN2 stands out of these materials due to the combination of its high heat capacity, light weight, low cost, and environmental safety. Solid neon (SNe), with a good heat capacity, is not a practical candidate because it is about 500 times more expensive than SN2. Liquid hydrogen (LH2), with melting point at 13.8 K and boiling point at 20.3 K in the right range, is another potential good competitor to SN2. However, in case of a magnet quench, the release of a large amount of gaseous hydrogen can put hospitals in extreme hazard. Thus, LH2 is an unsuitable cryogen for MRI magnets.

In the presence of SN2, an MRI magnet is more thermally stable than a conduction-cooled “dry” magnet. And more importantly, in the event of a power outage, SN2, an effective thermal reservoir, could keep the temperature of the magnet within its operating range for a certain period [31,32].

2.4. Switch design

Because of a relatively slow normal zone propagation speed in MgB_2 wire, this magnet ought to be actively protected. A detect-and-activate-the-heater technique was employed to protect this magnet [33].

As a major innovation of the magnet, we combined the switching and energy-absorbing functions into a single unit—a modified PCS. A circuit diagram of this design concept is shown in Figure 6. To charge or discharge the magnet, we open all 8 PCS’s as usual. When a quench is detected in the magnet, an insulated-gate bipolar transistor sends a current to the PCS heaters to heat up the PCS’s. Because the total PCS resistance is much larger than the resistance of an initial quench spot, most of the magnetic energy will be dumped into the PCS’s. In this design, we do not need separate energy absorbers or cumbersome protection heaters: each PCS has its own heater for both switching and protection. In addition, each PCS is thermally isolated from the cryogenic environment, enabling each PCS to be heated

more easily and promptly than sections of coils that are exposed to SN2, resulting in an efficient active protection procedure.

In order to absorb the entire magnetic energy while keeping PCS temperature <200 K, the total length of MgB_2 wire in all the PCS's needs to be >22 m. When quench triggered, the PCS's need to soak up the magnetic energy not only safely, but also promptly. According to an L-R circuit model equivalent to the magnet-PCS circuit, the necessary wire length to give a large enough resistance and thus a short enough time constant of ~5 s should be >156 m [27].

For normal switching function, all the energy to open the PCS's will stay in the cryogenic environment and eventually need to be taken away by a cryocooler. It means that the heat to open the PCS's ought to be minimized. For each PCS, this energy is simply its enthalpy difference between 10 K and 40 K. Thus, a smaller wire volume, e.g., a shorter wire length is desired for each PCS to minimize the energy. In the magnet, a total length of 80 m of MgB_2 wire was wound in the PCS's, namely, 10 m wire in the PCS of each coil module. When opened, the PCS's provided a current-decay time constant of ~10 s. Due to the presence of SN2, the time constant has been analytically justified for prompt quench protection [27].

As the volume of a PCS is usually small, its energy absorbing capacity is limited. Therefore, this protection technique works more practically for dedicated MRI magnets than whole-body MRI magnets, as the latter typically store much more magnetic energy than the former. For whole-body MRI magnets, conventional passive protection technique may be preferred.

2.5. Coil fabrication

Each coil was wound on a stainless steel mandrel using a winding machine. A 10 m length of wire was left at the beginning of winding for the PCS and joint. During winding, a 10-N winding tension was maintained in the wire to make the turns tight. After all the turns were wound in the winding groove, a PCS former was bolted on the side of the coil mandrel. Another 10 m length of wire was left at the end of winding before the wire was cut, again for the PCS and joint.

Each PCS was non-inductively wound. The two terminal wires of each coil were wound on a PCS former in opposite directions so that the magnetic field generated by the current was essentially canceled out. The PCS inductance, deduced from the drift of a small superconducting loop, was ~10 μH. The wires from the PCS were then terminated with a superconducting joint.

After a coil and its PCS were wound and terminals were spliced, the entire coil-PCS-joint module was heat treated in a box furnace at 700° C for 90 minutes in an argon environment. After heat treatment, the PCS was thermally insulated with 12-mm thick Styrofoam pieces. Two pieces of Manganin wire, each of 30 Ω, were embedded in the PCS as its heaters. Two thermocouples were also implanted in the PCS to monitor its temperature. Two thin copper strips were soldered to the coil as terminal lugs that were later used to connect adjacent coils with jumpers bolted to the lugs. Thereafter, the joint and not-well-secured wire sections

were epoxied to the mandrel with Stycast 2850 and hardener 24LV so that they could withstand Lorentz forces when the magnet was energized. Epoxying the parts also prevented accidental damage to the coil during subsequent handling.

All the 8 modules were successfully fabricated with the wind-and-react procedure described above. They were then assembled in the designed order and secured with aluminum beams and threaded rods. The assembly is shown in Figure 7(a). A thin layer of G-10 sheet, inserted at each contact between the magnet and the aluminum beams, electrically insulated the magnet from the rest of the system.

2.6. Test rig

A test rig was built for operation of the assembled magnet in SN2. Figure 7(b) shows the assembled test rig before it was inserted into a 432-mm-bore cryostat for testing.

The cooling subsystem provided cooling power to the magnet and kept it in the operation temperature range of 10–13 K. The major cooling source was a 2-stage GM cryocooler. According to its performance data, the 2nd stage cold head of the cryocooler provides cooling power of 8 W and 15 W, respectively, at 10 K and 18 K, enough for this magnet to operate in persistent mode over this temperature range.

During magnet ramp-up while all the 8 PCS's were open, the system had an additional heating load of 6 W that would overload the cooling capacity of the 2nd stage cold head. Thus, LHe was deployed as an effective but inefficient cooling source and forced through a cooling coil that was wound from a 12.7-mm diameter copper tube. The 36-turn cooling coil was tightly inserted in the magnet bore, as shown in Figure 7(c). Two stainless steel tubes, each of 0.25-mm thick wall and 12.7-mm diameter, were soldered to both ends of the copper tube as an inlet and an outlet. The thin-walled stainless steel tubes reduced conductive heat input from the top flange at approximately room temperature to the cryogenic environment.

This magnet, surrounded by a volume of SN2, was not directly conduction-cooled. During operation, however, four OFHC copper bars, inserted in the SN2, helped conduct heat away from the magnet through SN2. These copper bars, each 610-mm long, 51-mm wide and 3-mm thick, were thermally linked to the 2nd stage cold head and served as extended heat sinks in the SN2. With a total cross-sectional area of 612 mm^2, they were sufficient to carry 1 W of heat away over the length of 610 mm with a temperature difference of <1 K.

A pair of current leads was designed to carry 100-A current from the room temperature environment to the cryogenic environment with heat input within the cold head cooling capacity. Each lead consisted of two segments: an upper segment of copper bands and a lower segment of brass-HTS hybrid lead. The two segments were joined at and thermally anchored to the 1st stage cold head. The upper copper bands were optimized to carry 100 A while introducing only 2.4 W conductive heat to the 1st stage cold head. The brass-HTS hybrid leads were optimized to bring only 0.1 W conductive heat to the 2nd stage cold head. The Brass substrate of each lead was used as a heat sink and current shunt to the HTS tapes in case the HTS tapes failed.

3. Results and discussion

3.1. Solid nitrogen

In order to obtain crystalline rather than foamy SN2, liquid nitrogen (LN2) has to be solidified gradually. Nitrogen has a saturation liquid-to-solid phase transition at 63.16 K and 93.45 torr (0.122 atm). In this test, the following procedure was employed to solidify nitrogen, initially liquid at 77 K at 1 atm:

1. Fill 77-K LN2 into the cryostat;
2. Pump on the LN2 to cool LN2;
3. At 65 K, stop pumping and turn on the cryocooler to further cool down and solidify nitrogen.

Continuous pumping to its triple point could cause LN2 to solidify too fast and unevenly, forming foamy SN2 [34]. So, pumping was stopped at 65 K when nitrogen was still in liquid phase. With the cryocooler on, LN2 could solidify from the copper bars that were attached to the 2nd stage cold head and form crystalline SN2 (β-phase above 35 K and α-phase below 35 K). The cryocooler was able to cool 60-kg (~75 liters at 77 K) nitrogen from 65 K to 15 K in less than a week. Figure 10 shows cooling curves measured at different Cernox sensor locations. Two plateaus in the curves of C7 and C8 sensors—both inside SN2—at 63 K and 35 K, respectively, indicate the liquid-solid and solid-solid phase transitions of nitrogen. The cooling rates were 7×10^{-5} K/s during solidification and 2.5×10^{-4} K/s after solidification, slower than the cooling rate of 0.001 K/s used by Nakamura, et al, [34], guaranteeing crystalline SN2.

In the temperature range of 10–15 K, SN2 has a thermal conductivity of ~1 W/m·K that is much greater than those of other common insulating materials such as Kapton, Nylon or Mylar used in superconducting magnets [23]. The tails of the curves in Figure 10 shows that the temperature difference between the copper bars and the bottom of the magnet, when the temperature eventually stabled at ~15 K, was <1 K. Note that no thermally conductive (e.g., copper) connectors were placed between the coils and the heat sink, and only SN2 filled in the space and surrounded the magnet. SN2 was proven as an effective agent in making the magnet temperature uniform. Although copper has a thermal conductivity much larger than that of SN2 in the 10–15 K range, it can hardly be applied to each and every surface of a magnet, whereas SN2 can easily do so. A poor contact between a pair of surfaces may significantly impair the desired thermal conduction. Furthermore, the enthalpy changes for copper and SN2 from 10 K to 20 K are 280 kJ/m^3 and 4500 kJ/m^3, respectively. For the same volume, SN2 absorbs 16 times more thermal energy than copper does, making it a more capable and cost-effective temperature stabilizer than copper. Therefore, a combination of SN2 “bath” and extended copper heat sink—for example, the cryogenic design deployed in this magnet test setup—is an effective LHe-free cooling option for MRI magnets.

3.2. PCS operations in solid nitrogen

The opening and closing operations of the PCS’s in SN2 was found less prompt than the same operations in gaseous or liquid helium. Figure 11 shows temperature vs. time plots of a

PCS during a typical complete open-and-close cycle. PCS opening time depends on heating power; in our test, with 1-W heating power, a PCS was fully opened in ~10 minutes. After being fully opened, the PCS required a heating power of 0.7 W to maintain a temperature of >40 K in SN2, compared with heating powers of 1 W in gaseous helium and 3 W in LHe for the same operation [18]. It then took the PCS ~25 minutes to be fully closed in SN2, compared with a closing time of 3 minutes in gaseous helium [18]. To open a PCS in SN2, the SN2 surrounding the switch would be heated up, too. Similarly, the surrounding heated SN2 needed to be cooled before the PCS could be fully closed. So, the presence of SN2 meant a greater power and/or a longer period to a switch operation. In contrast, when a PCS was in gaseous helium, its surrounding helium was always replenished with cold helium vapor, making the PCS capable of being closed in a period of 3 minutes.

If a shorter opening/closing time is desired to operate an MRI magnet, a PCS/PCS's can be placed outside SN2, or inside SN2 but close to the cooling source, such as a cold head or a heat sink. A cooling source nearby a PCS would effectively suppress the warming up of the surrounding SN2, thus reducing its cooling time. Figure 12 illustrates a simplified 1-D model, in which a 12-mm layer of Styrofoam and a 50-mm layer of SN2 are sandwiched between a heated 50-K PCS and a 20-K heat sink. In the temperature range of 20–50 K, Styrofoam and SN2 have average thermal conductivities of 0.01 W/m·K and 0.4 W/m·K, respectively. At steady state, when the temperature distribution is fully developed in the Styrofoam and SN2, the temperature at the Styrofoam-SN2 interface is ~23 K. If the SN2 layer is shortened to 25 mm, the interface temperature will be reduced to ~21.5 K accordingly. Although the temperature change of SN2 is small, ~3 K in the thicker layer or ~1.5 K in the thinner layer, the associated enthalpy change is comparable to the enthalpy change of a PCS from 20 K to 50 K, due to the relatively large volume and heat capacity of SN2. Note that the enthalpy changes of SN2 from 20 to 23 K and steel from 20 to 50 K are 0.25×10^4 kJ/m^3 and 1×10^4 kJ/m^3, respectively. In this model, the enthalpy stored in the thinner SN2 layer is only ~1/4 of that in the thicker SN2 layer, which would certainly take less time to be conducted away while cooling the PCS.

3.3. Persistent-mode operation

The magnet was successfully ramped up and operated in persistent mode in the temperature range of 10–13 K. During the test, it sustained persistent center fields of 0.35 T at 70 A and 0.47 T at 100 A, with field decays <0.1 ppm/hour. For a magnet of an inductance of 0.74 H, this field decay rate requires a total resistance of $<2\times10^{-11}$ Ω in the magnet, e.g., $<2.5\times10^{-12}$ Ω in each joint. A typical superconducting joint made with monofilament unreacted MgB_2 wires has a resistance of $\ll3\times10^{-12}$ Ω [18], which meets the above requirement.

The magnet was first ramped up to 70 A at 13 K and sustained a nominal persistent field of 0.35 T for 7 days. Its measured center field, as shown in Figure 13, fluctuated around 0.350775±0.000075 T during a continuously monitored period of 120 hours (5 days). The field trace, though rising and dropping during the period, is not monotonic thus does not suggest any clear-cut field decay trend. Moreover, the axial field distribution mapped on the 1st day of persistent-mode operation matched that measured on the 7th day, reconfirming no decay along the z-axis. According to Figure 13, over this 120-hour period, the maximum and

minimum measured fields were 0.35085 T and 0.35070 T, respectively, indicating a temporal field variation of <3.5 ppm/hour. We believe that the field fluctuation was due to drift of the measuring system. The magnetic field was measured by a Hall sensor—the temperature of the sensor, the driving current to the sensor and the data acquisition system could all contribute to the drift of the final results. The field, however, never dropped below the initial value of 0.35070 T during the entire period, suggesting that the actual field decay should be <0.1 ppm/hour.

The magnet was further ramped up to 100 A at 9 K, generating a center field of 0.496 T. After an initial field settlement when temperature rose from 9 K to 12.5 K, the magnet was then able to keep its center field constant at 0.47050 T at ~12.5 K, as shown in Figure 15. The field trace kept nearly flat during the continuously monitored period of 50 hours, suggesting a field decay of <1 ppm/hour.

Throughout the entire tests, with multiple ramping up and persistent-mode operation sequences, there was no premature quench happened in the magnet. Flux jumping, a phenomenon that had stopped monofilament NbTi wires being applied to magnets, was deemed no long an active issue with monofilament MgB_2 wires.

3.4. Current distribution

When the magnet was ramped up to 100 A, the axial field profile at 9 K (open square), as illustrated in Figure 16, was initially homogeneous and similar to the 70-A persistent-mode field profile shown in Figure 14. The axial field distribution was distorted at higher temperatures as the field settled down. Figure 16 shows the nominal 100-A field profiles at 9 K and then at 13 K, and again after 2 days, at 13 K and 14 K. Note that even though the field profile got distorted when the temperature rose from 9 K to 13 K, the field afterwards remained persistent and the distorted field profile stayed unchanged, confirming superconductivity of the joints. Since the magnet had shown performance variation among coils, we decided to stop rising its operating temperature at 13 K.

The axial field profile became distorted, as each coil settled to its own persistent current level, i.e., at higher temperatures, a diverse performance among the coils became more distinct. The least squares method was employed to inversely calculate the current in each coil from the field profile. The field at each mapped point B_i is contributed from the 8 coils:

$$B_i = \sum_{j=1}^{8} C_{ij} I_j$$

or written in matrix form:

$$B = CI$$

Here, C_{ij} is the field generated at point i from Coil j at the unit current of 1 A, I_j is the actual current in Coil j. Here, the number of measured points $i = 25$, and the number of coils $j = 8$. Applying the least squares method, we obtained the current in each coil:

$$\hat{I}=(C^T C)^{-1} C^T B$$

The optimal current distribution solution $\hat{I}$ is summarized in Table 2. Coils 1–8 are labeled from top to bottom. With this current distribution, the calculated axial field profile perfectly matches the measured field distortion.

Theoretically, the currents in all the 8 coils should be the same during ramp up and remain constant after closing the PCS's and throughout persistent-mode operation. The field distortion of the magnet operated at 0.5 T at 13 K was due to a diverse performance among coils rather than the modular approach itself. Because each coil formed a complete superconducting loop, the self-inductance of a coil and mutual inductance between coils acted together to change the current in each coil. The coils with lower I_c's had their currents decay, which in turn increased the currents in the other coils via mutual inductance. We believe that Coils 1, 2, 5 and 6 with currents <100 A had lower wire or joint I_c's, while Coils 3, 4, 7 and 8 with induced currents >100 A had higher I_c's.

Operated at lower temperature or lower current, the coils should be completely superconducting and perform equally well. Specifically, the current sustained in each coil module should keep constant and equal to the current output from a power supply. In order to justify it, the magnet was ramped up to a lower current of 10 A at which no diverse performance among coils emerged. The axial field profiles both before and after closing the PCS's were mapped and compared, experimentally confirming this current persistency.

Figure 17 shows three sets of the magnet axial field mapping results at 10 A: 1) in driven mode when all the 8 PCS's were fully open (open squares); 2) in driven mode when all the 8 PCS's were fully closed (open circles); and 3) in persistent mode when the power supply was removed (triangles). A total of 25 points were mapped on the center z-axis, at a 20-mm increment. The 3 field profiles agree perfectly with each other, proving that the currents remained constant during the PCS operations and through the persistent-mode operation.

3.5. Protection

To verify that the PCS's were able to absorb the magnetic energy and thereby protect the magnet in a real quench, the PCS's protection function was tested in SN2. With the magnet in persistent mode at 100 A, all the PCS heaters were manually activated, giving 10 W to each PCS, to induce a dumping process. Figure 18 shows the center field and the temperature traces of the 8 PCS's recorded at the beginning of the dumping process. Note that at t = 25 s, 3 seconds after the PCS heaters being activated, the field started to decay. In 10 seconds of the triggered dump, the field decayed to half of its initial value, and in 25 seconds the field decayed almost entirely. After the magnetic energy being completely dumped, the temperature of each PCS remained below 70 K. A reaction time of 3 seconds was fast enough to protect the MgB_2 wire operated at 100 A [27]. And a maximum temperature of <70 K in the PCS's was considered safe from damages by thermal strain. After the test, the magnet was ramped up and kept at 50 A persistently at 15 K, verifying that the magnet was not damaged during the dumping process.

4. Conclusions

Persistent-mode operation was achieved with an MgB_2 magnet composed of 8 separate coil modules, each equipped with its own PCS and terminated with a superconducting joint.

Monofilament wire, once devastating for NbTi due to flux jumping, was deemed satisfactory for MgB_2. The high critical temperature of MgB_2 provided adequate energy margin for the magnet operated in the 10–13 K range and flux-jumping-free.

Because of the splicing technique, as well as the brittleness of MgB_2 wire, the wind-and-react procedure, well established with Nb_3Sn magnets, was adopted for the MgB_2 magnet. The costs and operations associated with the heat treatment of this magnet were deemed manageable.

Modularization has been proven viable with wind-and-react procedure for this magnet, as MgB_2 magnet technology has yet to reach the mature stage. It made operations—particularly heat treatment—more manageable and minimized the risk of damaging the entire magnet.

In the absence of a liquid helium bath, solid nitrogen considerably enhanced the thermal capacity of the cold mass, providing good thermal stability to the magnet. Solid nitrogen, due to its relatively large thermal conductivity at 10–13 K, also maintained a uniform temperature environment around the magnet.

The technology developed for this magnet can be scaled up for whole-body MRI magnets with certain trade-offs. Wind-and-react procedure, though unfavorable, can still be used to produce larger coils with higher cost. It will therefore enable the splicing technique that works well with monofilament MgB_2 wire. Modularization would barely work for whole-body MRI magnets, chiefly because of its multi-PCS concept. Solid nitrogen can be an effective thermal enhancer for MRI magnets and provide a long ride-through time. Its large thermal capacity may significantly extend the first cool down time, which can be taken care of in manufacturers' production facilities before shipment.

The completion of this persistent-mode MgB_2 magnet at the FBML, MIT may be considered a major milestone in the MgB_2 MRI magnet technology. It has proven that MgB_2 is a viable option for the next generation LHe-free MRI magnet system. We expect the success of this magnet to promote further R&D works in this technology and to eventually result in readily available MRI medical care everywhere, here and particularly in developing countries.

Acknowledgments

This work was supported by the National Institute of Biomedical Imaging and Bioengineering of the National Institute of Health under Award Number R01EB002887.

References

1. U.S. Geological Survey. Mineral Commodity Summaries. 2000–2016
2. Nagamatsu J, Nakagawa N, Muranaka T, Zenitani Y, Akimitsu J. Superconductivity at 39 k in magnesium diboride. Nature. 2001; 410(6824):63–64. [PubMed: 11242039]

3. Stenvall A, Hiltunen I, Korpela A, Lehtonen J, Mikkonen R, Viljamaa J, Grasso G. A checklist for designers of cryogen-free MgB_2 coils. Supercond Sci Technol. 2007; 20:386–391.
4. Zhang D, et al. Research on MgB_2 superconducting magnet with iron core for MRI. IEEE Trans Appl Supercond. 2010; 20(3):764–768.
5. Zhang D, et al. Research on stability of MgB_2 superconducting magnet for MRI. IEEE Trans Appl Supercond. 2011; 21(3):2100–2103.
6. Li, Xiao Hang, Du, Xiao Ji, Bao, Qing, Kong, Ling Qi, Ye, Li Yang, Xiao, Li Ye. Design, development and experiment of a 1.5 T MgB_2 superconducting test magnet. Cryogenics. 2009; 49:286–90.
7. Li, Xiaohang, et al. A small 1.5 T persistent current operating test magnet using MgB_2 wire with high J_c joints. IEEE Trans Appl Supercond. 2011; 21(3):1616–1619.
8. Mine, Susumu, Xu, Minfeng, Buresh, Steve, Stautner, Wolfgang, Immer, Christopher, Laskaris, Evangelos T., Amm, Kathleen. Development of a compact 3 T MgB_2 magnet. IEEE Trans Appl Supercond. 2014; 24(3):4400404.
9. Mine, Susumu, Xu, Minfeng, Bai, Ye, Buresh, Steve, Stautner, Wolfgang, Immer, Christopher, Laskaris, Evangelos T., Amm, Kathleen. Development of a 3 T-250 mm bore MgB_2 magnet system. IEEE Trans Appl Supercond. 2015; 25(3):4600604.
10. Razeti, Marco, Angius, Silvano, Bertora, Leonardo, Damiani, Daniele, Marabotto, Roberto, Modica, Marco, Nardelli, Davide, Perrella, Mauro, Tassisto, Matteo. Construction and operation of cryogen free MgB_2 magnets for open MRI systems. IEEE Trans Appl Supercond. 2008; 18:882–886.
11. Modica M, Angius S, Bertora L, Damiani D, Marabotto M, Nardelli D, Perrella M, Razeti M, Tassisto M. Design, construction and tests of MgB_2 coils for the development of a cryogen free magnet. IEEE Trans Appl Supercond. 2007; 17:2196–2199.
12. Yao, Weijun, Bascuñán, Juan, Kim, Woo-Seok, Hahn, Seungyong, Lee, Haigun, Iwasa, Yukikazu. A solid nitrogen cooled MgB_2 "demonstration" coil for MRI applications. IEEE Trans Appl Supercond. 2008; 18(2):912–915. [PubMed: 20390056]
13. Yao, Weijun, Bascuñán, Juan, Hahn, Seungyong, Iwasa, Yukikazu. A superconducting joint technique for MgB_2 round wires. IEEE Trans Appl Supercond. 2009; 19(3):2261–2264. [PubMed: 20671806]
14. Yao, Weijun, Bascuñán, Juan, Hahn, Seungyong, Iwasa, Yukikazu. MgB_2 coils for MRI applications. IEEE Trans Appl Supercond. 2010; 20(3):756–759.
15. Park, Dong Keun, Ling, Jiayin, Rindfleisch, Matt, Voccio, John, Hahn, Seungyong, Bascuñán, Juan, Tomsic, Michael, Iwasa, Yukikazu. MgB_2 for MRI magnets: Test coils and superconducting joints results. IEEE Trans Appl Supercond. 2012; 22(3):4400305.
16. Ling, Jiayin, Voccio, John, Kim, Youngjae, Hahn, Seungyong, Bascuñán, Juan, Park, Dongkeun, Iwasa, Yukikazu. Monofilament MgB_2 wire for a whole-body MRI magnet: Superconducting joints and test coils. IEEE Trans Appl Supercond. 2013; 23(3):6200304.
17. Ling, Jiayin, Voccio, John P., Hahn, Seungyong, Kim, Youngjae, Song, Jungbin, Bascuñán, Juan, Iwasa, Yukikazu. Development of a 0.5-T/240-mm MgB_2 MRI Magnet: Assembly Design and Module Coils. IEEE Trans Appl Supercond. 2014; 24(3): 4400805.
18. Ling, Jiayin, Voccio, John P., Hahn, Seungyong, Kim, Youngjae, Song, Jungbin, Bascuñán, Juan, Iwasa, Yukikazu. Construction and Persistent-Mode Operation of MgB_2 Coils in the Range 10–15 K for a 0.5-T/240-mm Cold Bore MRI Magnet. IEEE Trans Appl Supercond. 2015; 25(3): 4601705.
19. Hales PW, Milward S, Harrison S, Jones H. A Solid-Nitrogen Cooled High-Temperature Superconducting Magnet for use in Magnetohydrodynamic Marine Propulsion. IEEE Trans Appl Supercond. 2006; 16:1419–1422.
20. Halesa P, Jonesa H, Milwardb S, Harrisonb S. Investigation into the use of solid nitrogen to create a "Thermal Battery" for cooling a portable high-temperature superconducting magnet. Cryogenics. Feb; 2005 45(2):109–115.
21. Wang Q, Dai Y, Song S, Wen H, Bai Y, Yan L, Kim K. A 30 kJ Bi2223 High Temperature Superconducting Magnet for SMES with Solid-Nitrogen Protection. IEEE Trans on Appl Supercond. 2008; 18:754–757.

22. Iwasa, Yukikazu, Bascuñán, Juan, Hahn, Seungyong, Park, Dong Keun. Solid-Cryogen Cooling Technique for Superconducting Magnets of NMR and MRI. Physics Procedia. 2012; 36:1348–1353.
23. Iwasa, Yukikazu. Case Studies in Superconducting Magnets - Design and Operational Issues. 2. Springer; 2009.
24. Lvovsky Y, Jarvis P. Superconducting systems for MRI—present solutions and new trends. IEEE Trans Appl Supercond. Jun; 2005 15(2):1317–1325.
25. Lvovsky Y, Stautner EW, Zhang T. Novel technologies and configurations of superconducting magnets for MRI. Superconductor Science and Technology. 2013; 26:093001, 71.
26. Cosmus TC, Parizh M. Advances in Whole-Body MRI Magnets. IEEE Transactions on Applied Superconductivity. 2011; 21:2104–2109.
27. Ling, Jiayin. PhD thesis. Department of Mechanical Engineering, M.I.T; Cambridge, MA: Feb. 2016 A persistent-mode MgB_2 0.5-T/240-mm Solid-Nitrogen-Cooled Magnet for MRI.
28. Ling, Jiayin. Master thesis. Department of Mechanical Engineering, M.I.T; Cambridge, MA: Sep. 2012 Monofilament MgB_2 Wires for MRI Magnets.
29. Li GZ, Yang Y, Susner MA, Sumption MD, Collings EW. Critical current densities and n-values of MgB_2 strands over a wide range of temperatures and fields. Supercond Sci Technol. 2012; 25:025001.
30. Li, Guangze, Zwayer, Jake B., Kovacs, Chris J., Susner, Michael A., Sumption, Michael D., Rindfleisch, Matthew A., Thong, Chee J., Tomsic, Michael, Collings, Edward W. Transport critical current densities and n-values of multifilamentary MgB_2 wires at various temperatures and magnetic fields. IEEE Trans Appl Supercond. 2014; 24(3):6200105.
31. Haid, Benjamin J. PhD thesis. Massachusetts Institute of Technology; Jun. 2001 A “permanent” high-temperature superconducting magnet operated in thermal communication with a mass of solid nitrogen.
32. Haid, Benjamin J., Lee, Haigun, Iwasa, Yukikazu, Oh, Sang-Soo, Kwon, Young-Kil, Ryu, Kang-Sik. Design analysis of a solid heat capacitor cooled “permanent” high-temperature superconducting magnet system. Cryogenics. 2002; 42:617.
33. Park, Dong Keun, Hahn, Seungyong, Bascuñán, Juan, Iwasa, Yukikazu. Active protection of an MgB_2 test coil. IEEE Trans Appl Supercond. 2011; 21(3):2402. [PubMed: 22081754]
34. Nakamura T, Muta I, Okude K, Fujio A, Hoshino T. Solidification of nitrogen refrigerant and its effect on thermal stability of HTSC tape. Physica C. 2002:1434–1437.

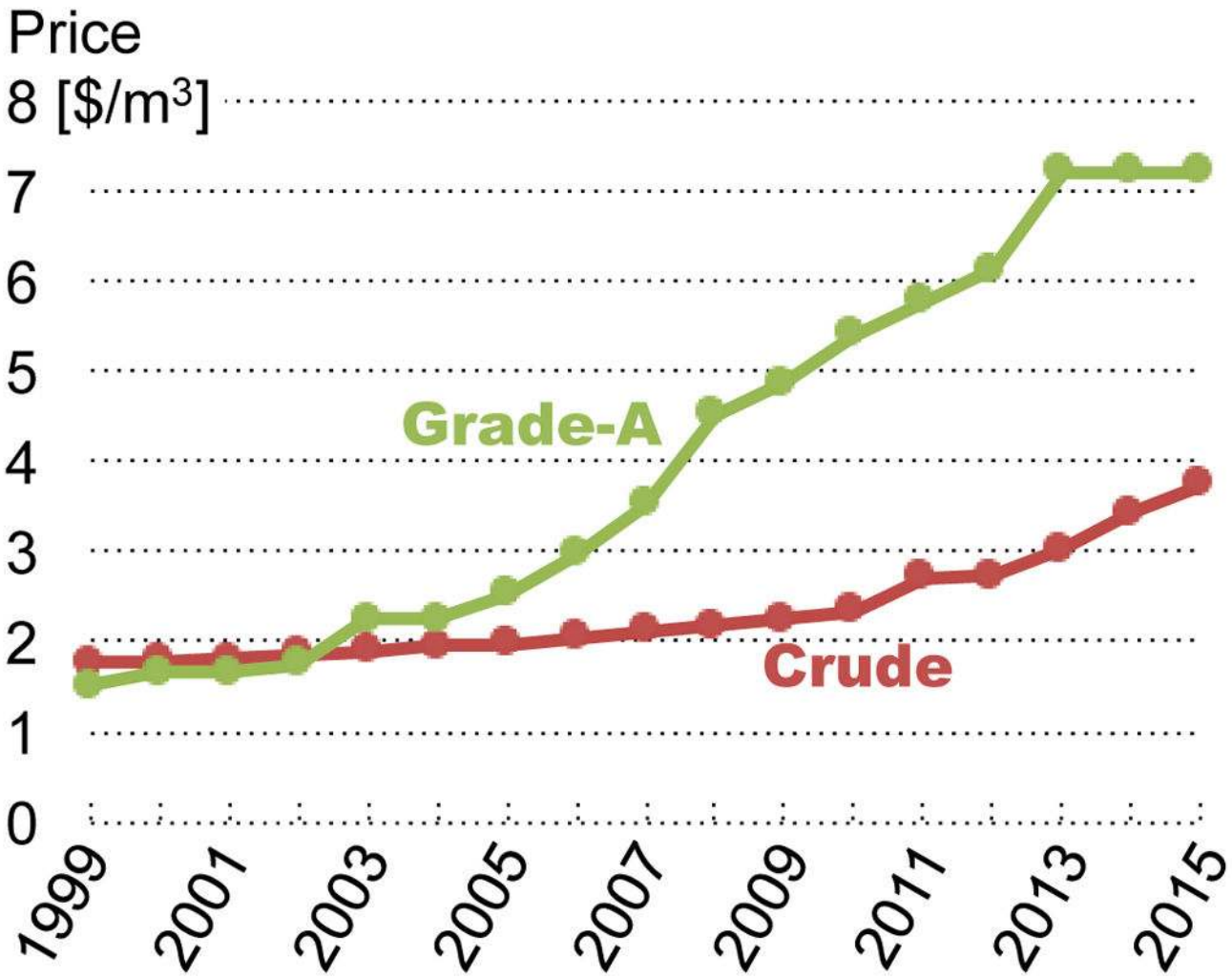

Figure 1.
Price of gaseous helium in the US plotted vs. year in 1999–2015 [1].

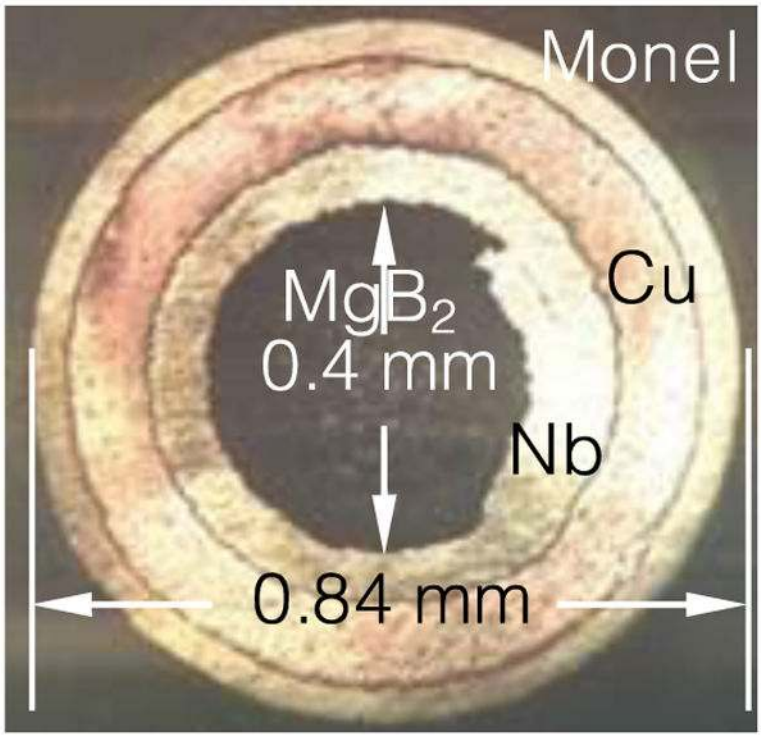

Figure 2.
MgB_2 wire cross-section. (Photograph courtesy of Hyper Tech Research.)

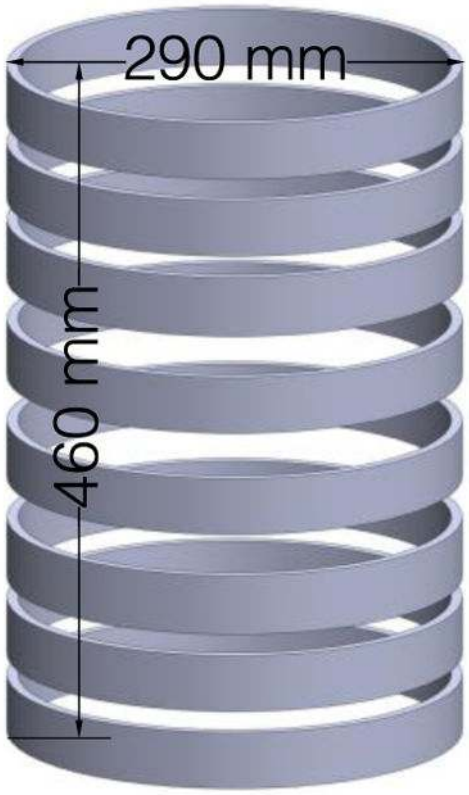

Figure 3.
Schematic drawing of MgB_2 magnet composed of 8 MgB_2 coil modules.

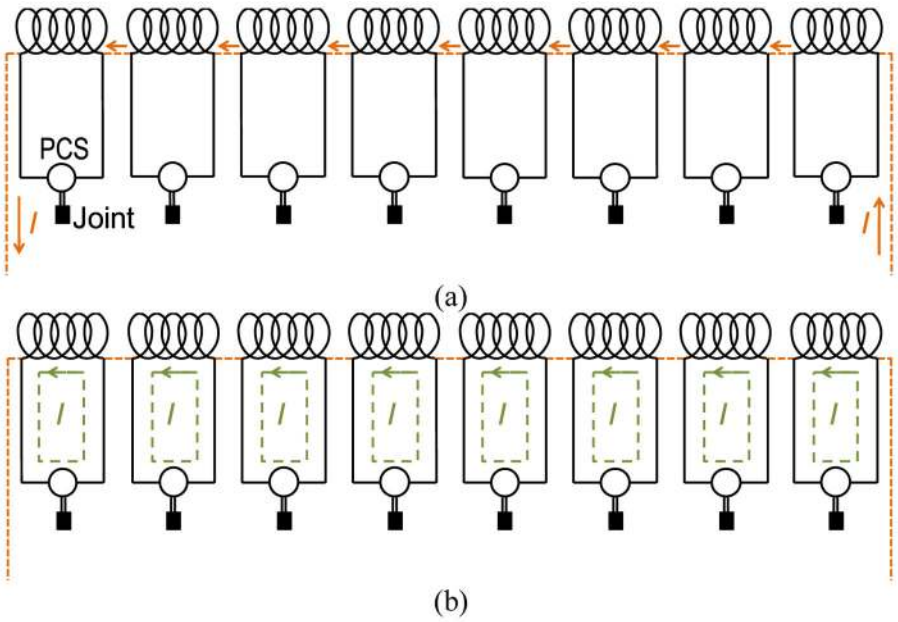

Figure 4.

Circuit diagrams of 8 coil modules connected in series. Dashed orange lines indicate resistive leads. Each circle indicates a PCS in each coil module. A small dot below each circle indicates a superconducting joint. (a) PCS's open, the coil modules may be charged all at once. (b) PCS's closed, persistent current loops (dashed green lines) may be sustained in coils.

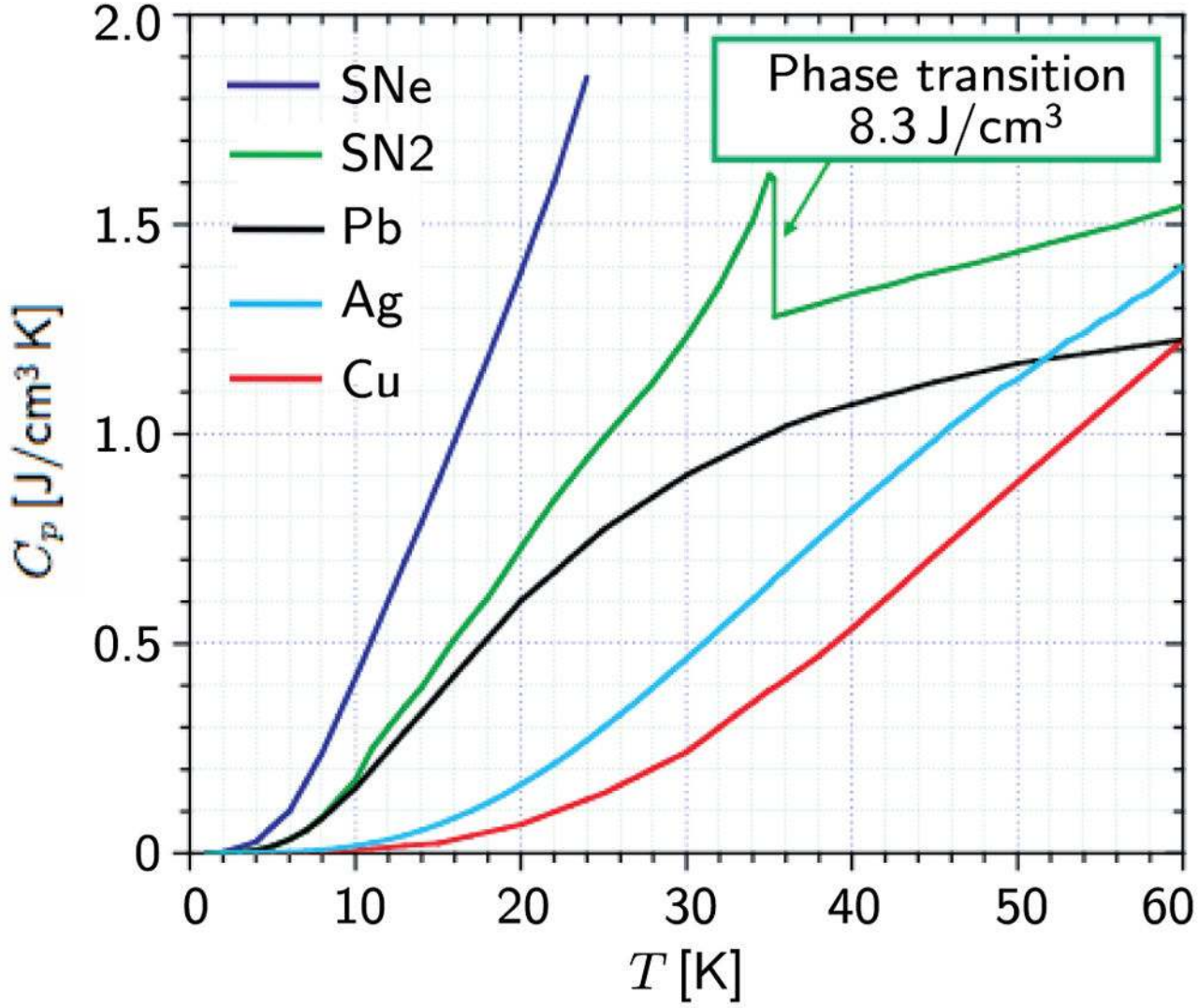

Figure 5.
Heat capacities of major cryogenic materials, e.g., solid neon (SNe), solid nitrogen (SN2), lead, silver, and copper, at cryogenic temperature [23].

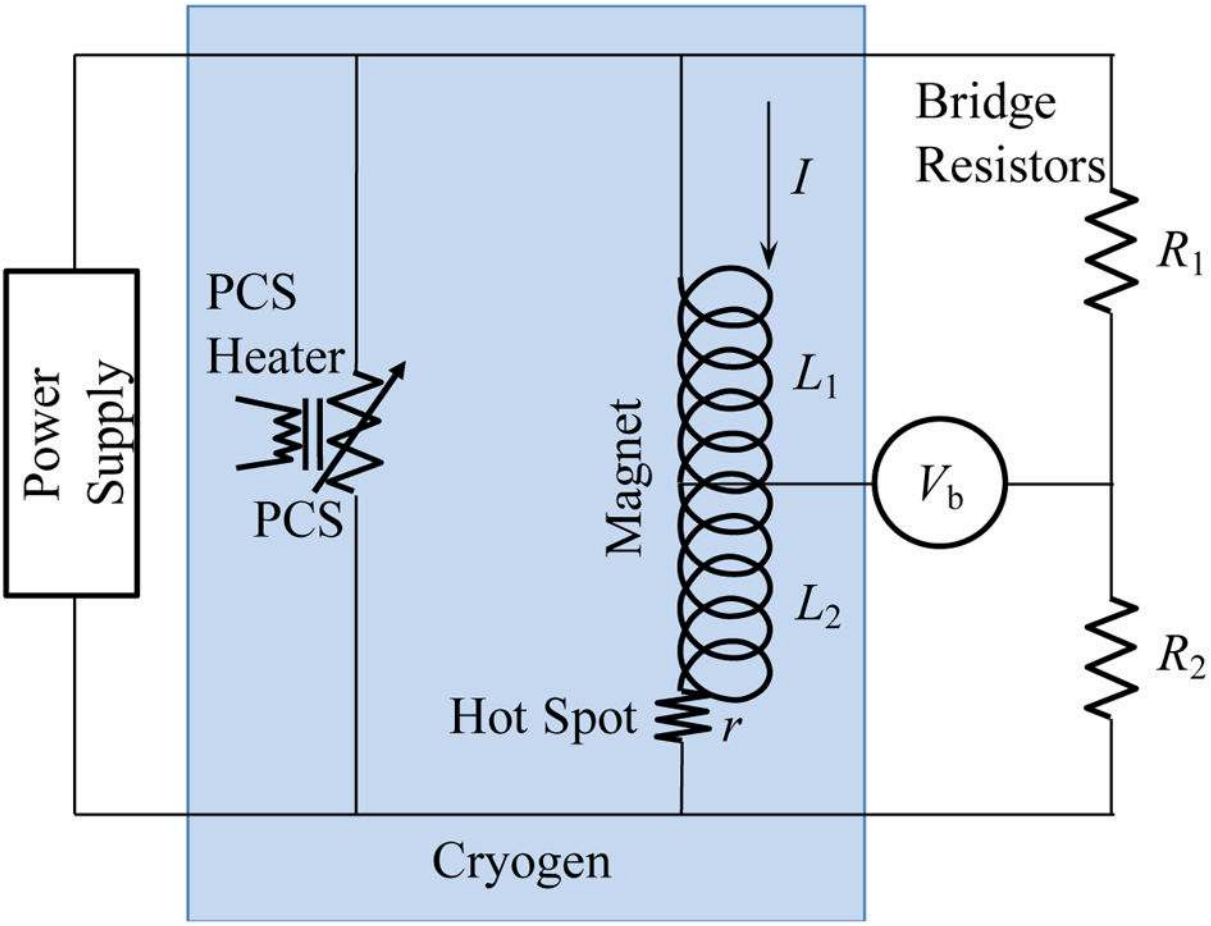

Figure 6.
Circuit diagram of a detect-and-activate-the-heater protection concept with PCS as the energy absorber.

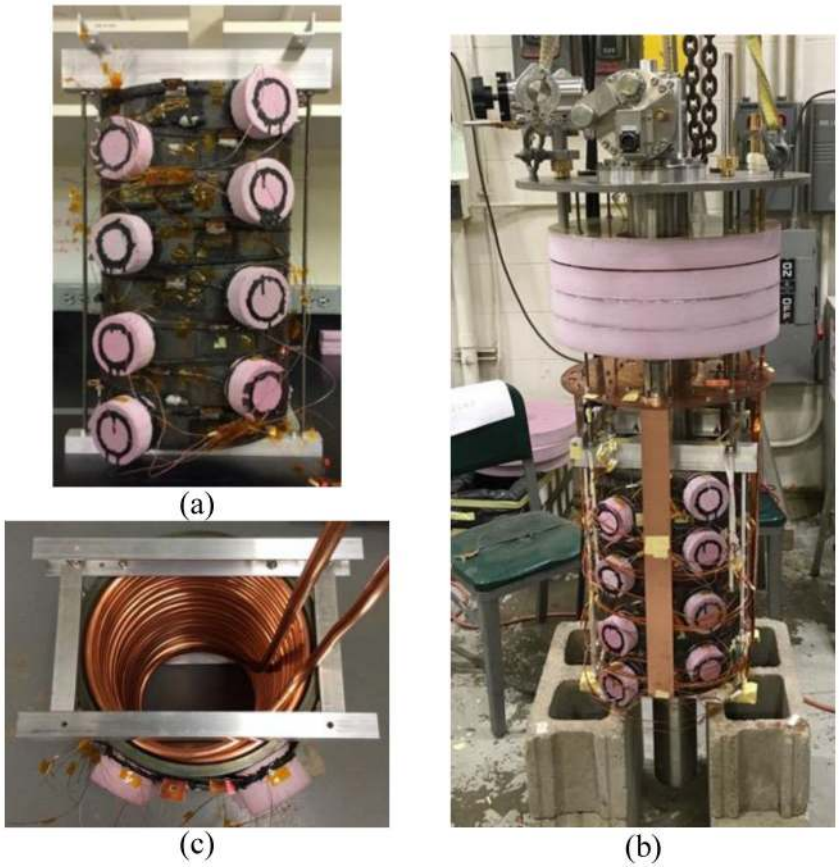

Figure 7.

Photos of the magnet. (a) Photo of 8-coil magnet fastened with aluminum beams and threaded rods. (b) Photo of assembled test rig for persistent-mode operation in SN2. (c) Photo of copper cooling coil in magnet bore.

Figure 8.
Brass-HTS hybrid leads, YBCO conductors soldered on brass bars.

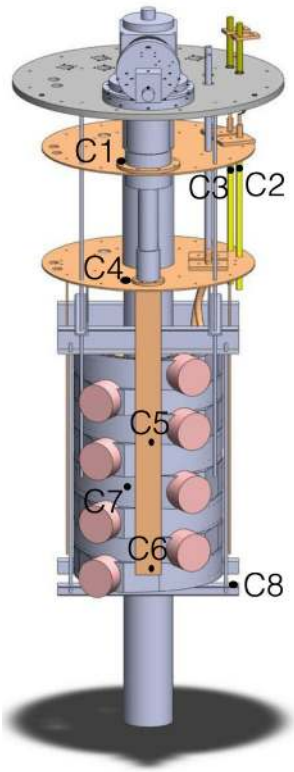

Figure 9.

Locations of 8 Cernox sensors. C1: 1st-stage cold head; C2: positive current lead; C3: negative current lead; C4: 2nd-stage cold head; C5: heat sink middle; C6: heat sink bottom; C7: magnet middle; C8: magnet bottom.

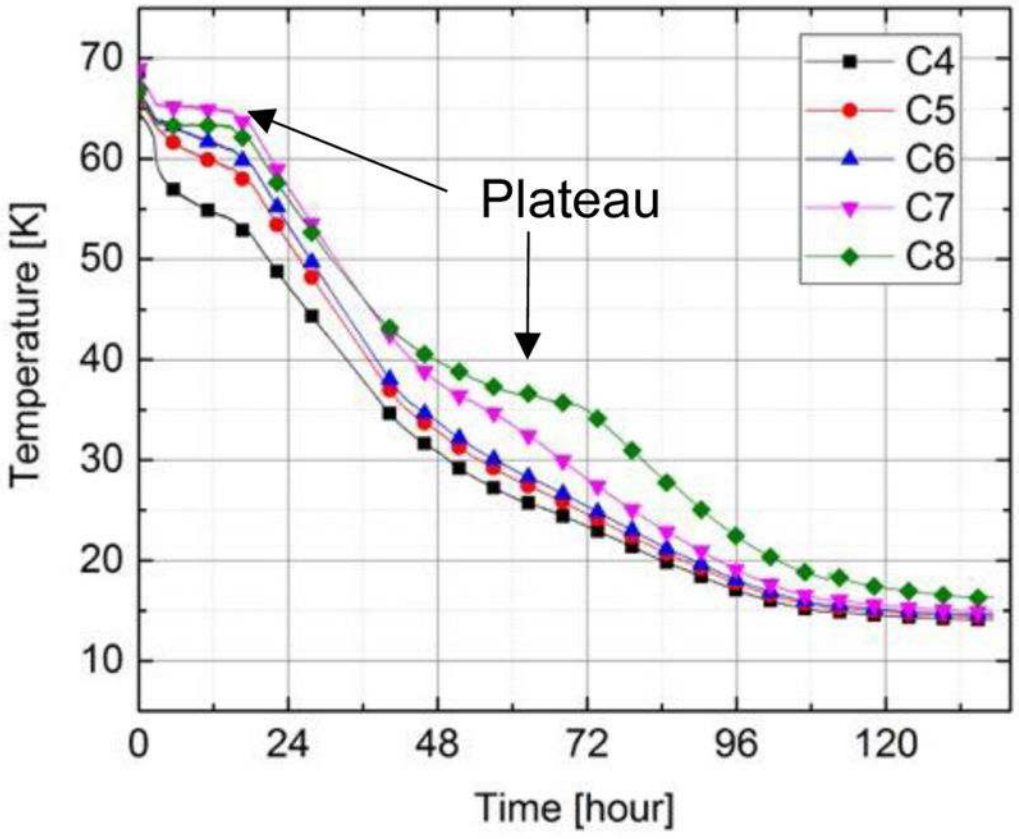

Figure 10.
Measured SN2 temperature vs. time plots, from ~65 K to ~15 K, cooled by cryocooler.

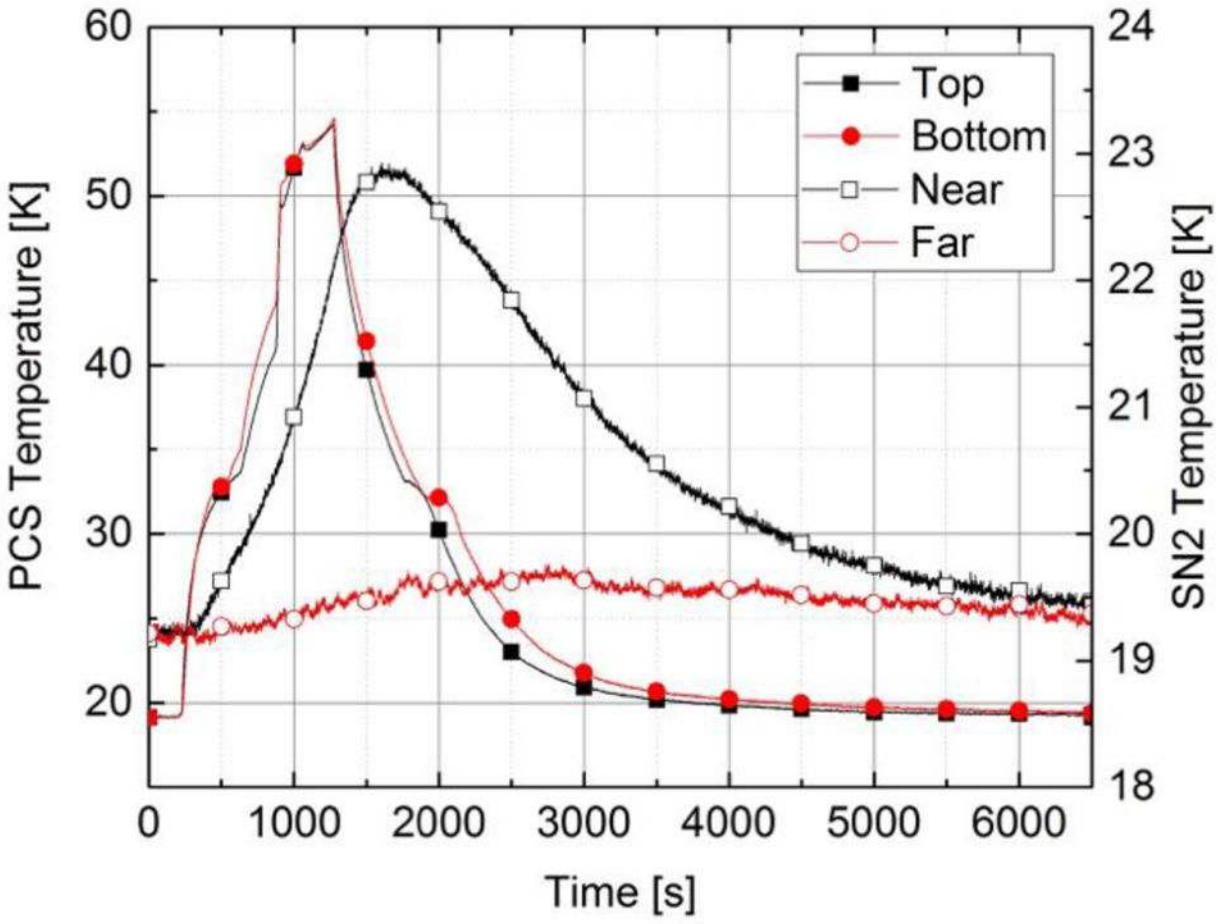

Figure 11.

Temperature vs. time plots of PCS opening/closing operation in SN2 at 19 K. Temperatures measured inside PCS of lowest coil, at the top (solid square) and bottom (solid circle), and outside the PCS, ~1 cm (open square) and ~10 cm (open circle) away.

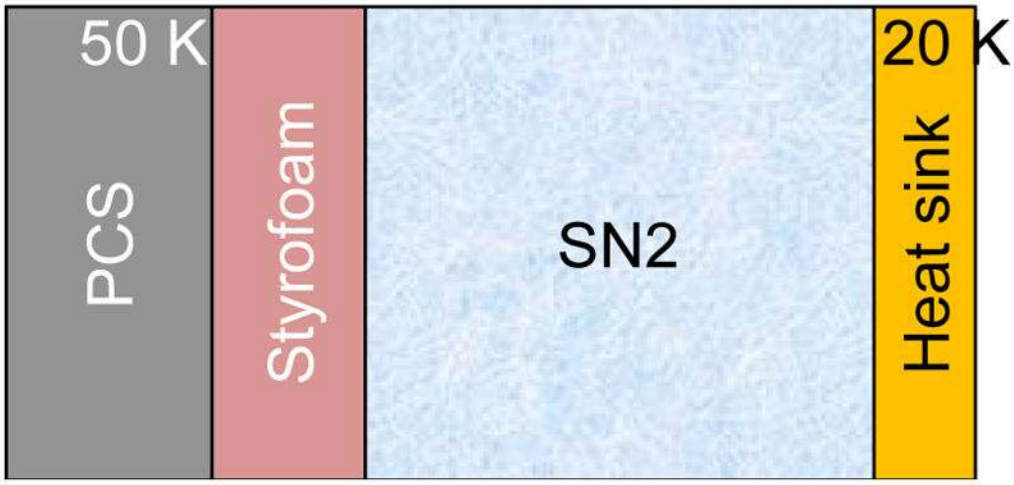

Figure 12.
Sketch of 1-D model of PCS operation in SN2.

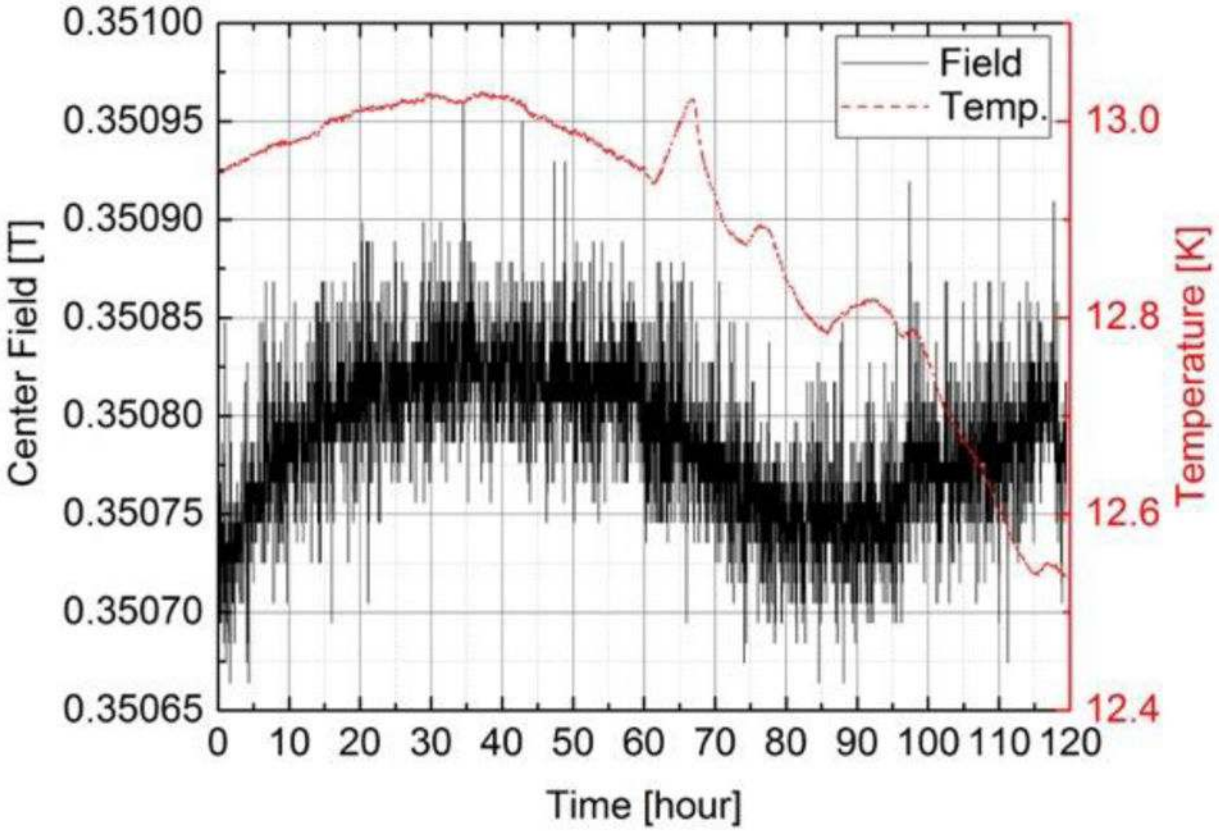

Figure 13.
Center field and temperature vs. time plots at 70 A.

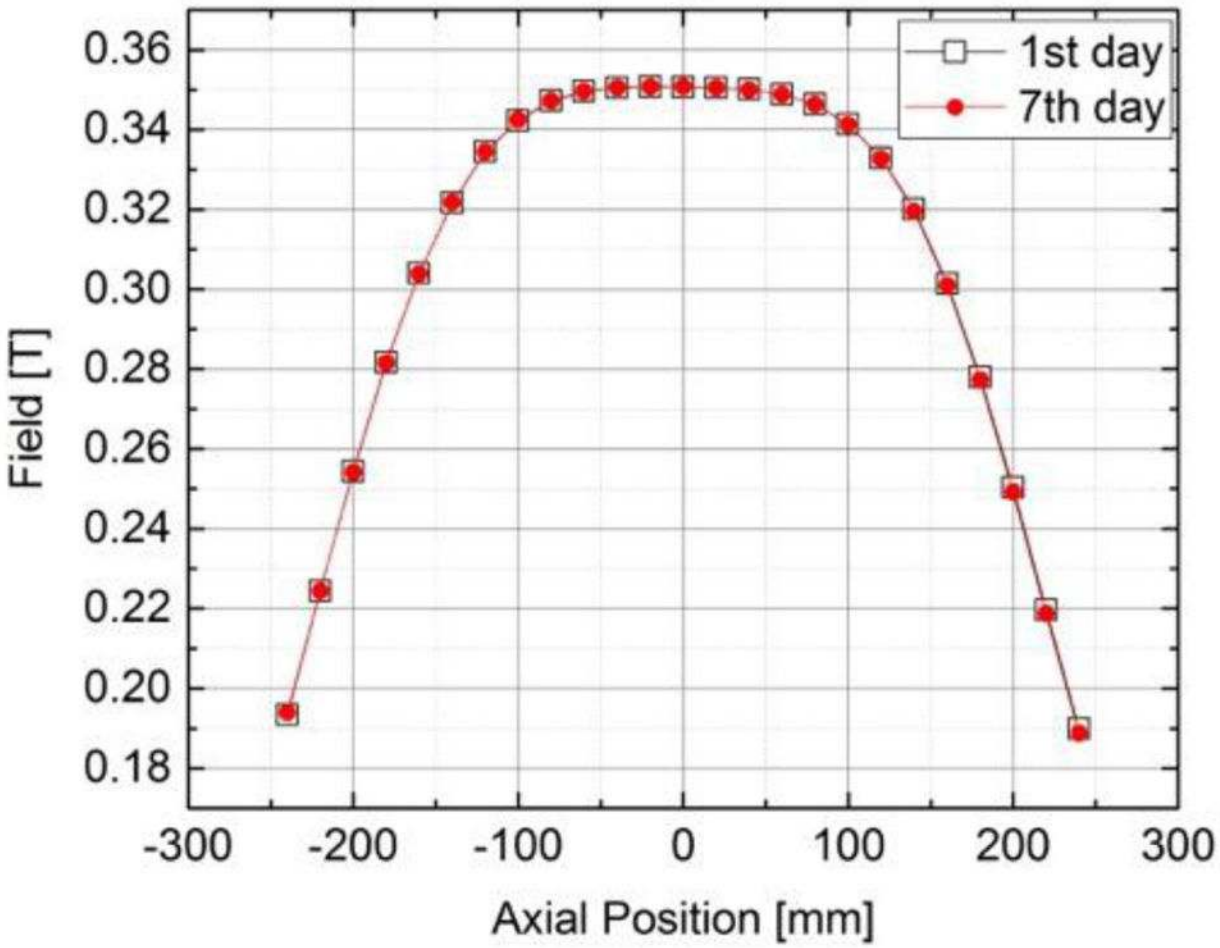

Figure 14.
Axial field profiles mapped on 1st and 7th days while a center field of 0.35 T remained persistent.

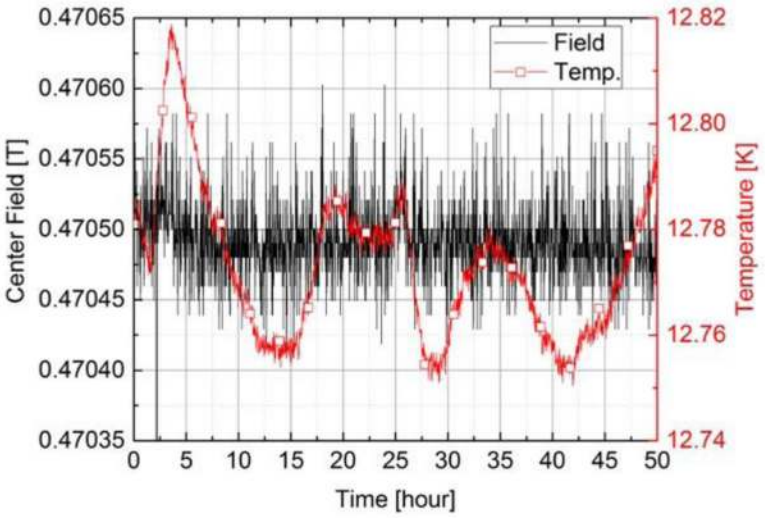

Figure 15.
Center field and temperature vs. time plots in persistent mode at nominal 100 A at 13 K.

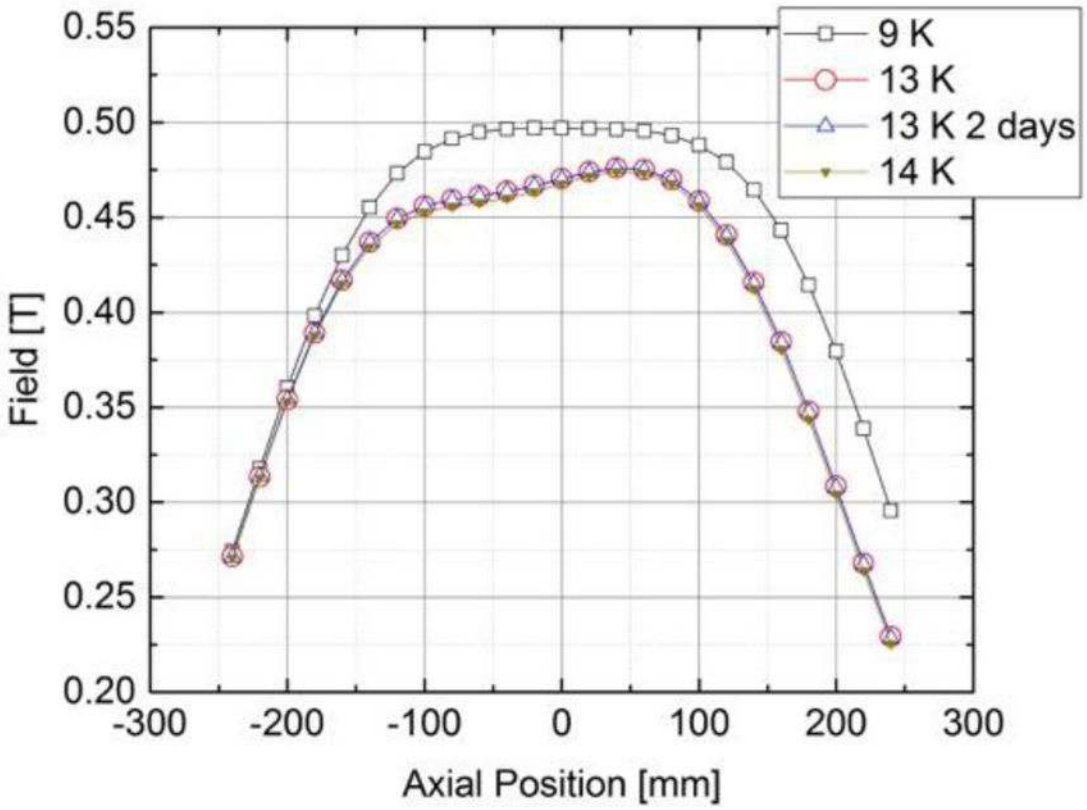

Figure 16.

Four sets of axial field mapping results, at nominal 100 A, of the magnet: 1) black squares, at 9 K, no field distortion; 2) red circles, at 13 K, some field distortion; 3) blue triangles, at 13 K for two days, constant distortion; and 4) yellow triangles, at 14 K, constant distortion.

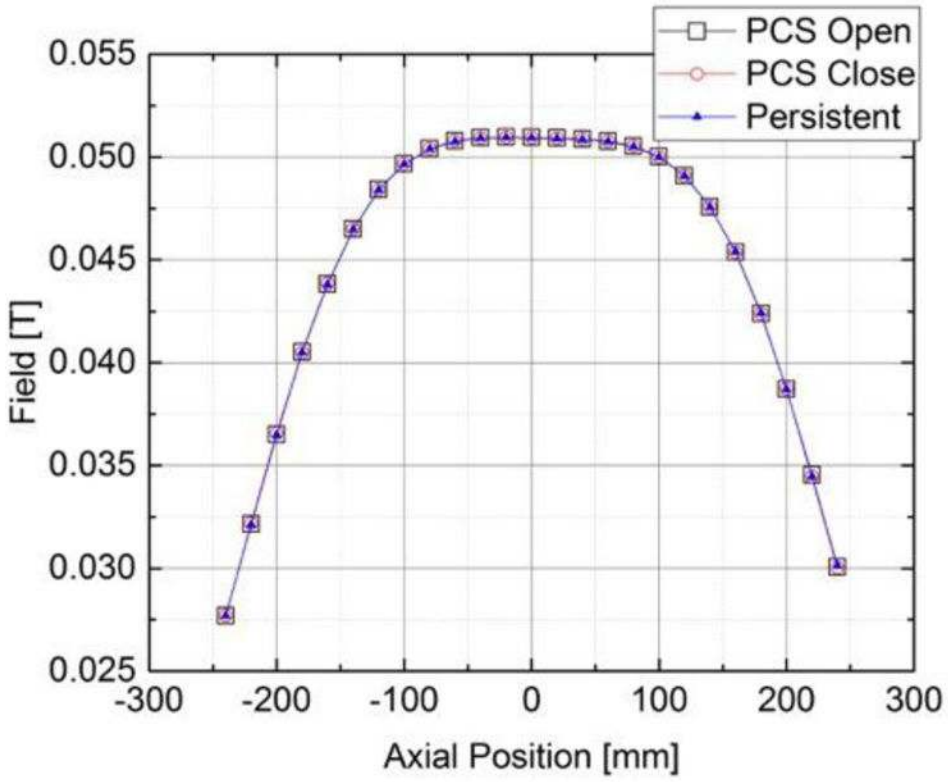

Figure 17.

Three sets of axial field mapping results, at 10 A, of the magnet: 1) black squares, in driven mode with each PCS open; 2) red circles, in driven mode with each PCS close; and 3) blue triangles, in persistent mode.

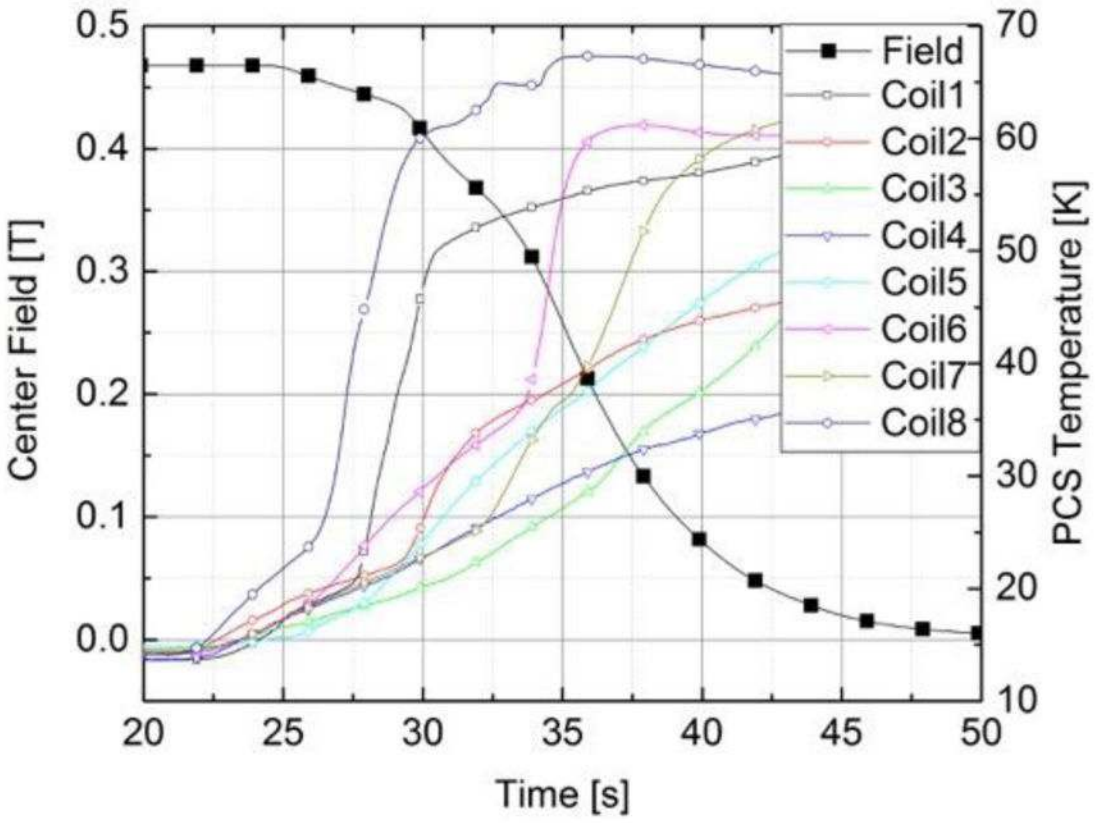

Figure 18.
Center field and 8-PCS temperatures vs. time plots during the first 30 s of a manually-induced dumping process.

Table 1

Key Electromagnetic Parameters

PARAMETERS [UNIT]	VALUES
Inner Diameter [mm]	276
Outer Diameter [mm]	290
Total Height [mm]	460
Total Number of Turns	2336
Single conductor Length [m]	<300
Total Conductor Length [km]	2.1
Total Magnet Mass [kg]	40
Operating Current [A]	102
Center Field @ 102 A [T]	0.5
Peak Field @ 102 A [T]	0.7
Inductance [H]	0.74
Total Magnetic Energy @ 102 A [kJ]	3.7
Overall Current Density [MA/m^2]	113
Field Error in 12-cm DSV [ppm]	<200

Table 2

Computed Current in Each Coil at 0.47 T [A]

Coil 1	*Coil 2*	*Coil 3*	*Coil 4*	*Coil 5*	*Coil 6*	*Coil 7*	*Coil 8*
48	78	115	110	77	77	105	105